

THE HIGHLY COLLIMATED BIPOLAR OUTFLOW NGC 2264G

Charles J. Lada

Smithsonian Astrophysical Observatory, 60 Garden Street, Cambridge, MA 02138, USA

and

Michel Fich

Physics Department, University of Waterloo, Waterloo, Ontario, Canada N2L 3G1

RESUMEN

En este trabajo presentamos una revisión de un estudio observacional detallado de la emisión de CO del espectacular flujo molecular bipolar NGC 2264G. Estas observaciones muestran un rico detalle estructural tanto en la morfología espacial como en el campo de velocidades del flujo. El campo de velocidades puede ser descrito con gran precisión por una ley de "Hubble" sobre toda la extensión del flujo bipolar. Las características generales del campo de velocidades y de la forma del lóbulo rojo sugieren la presencia de una onda de choque en forma de arco propagándose en un medio con un gradiente de densidad decreciendo hacia afuera. Sobre todo, las observaciones del campo de velocidad espacial de los dos lóbulos del flujo bipolar sugieren que el agente conductor del gas molecular es un chorro energético y rápido que surge de la fuente protoestelar central. Las notables asimetrías en la distribución del material de baja velocidad en los dos lóbulos sugieren una asimetría intrínseca en la estructura del gas ambiente en el cual el flujo bipolar se está propagando. Los valores que se obtienen de la masa, tamaño y energía del flujo imponen fuertes restricciones en la fuente conductora.

ABSTRACT

In this contribution we present an overview of a detailed observational study of CO emission from the spectacular bipolar molecular outflow NGC 2264G. These observations reveal rich structural detail in both the spatial morphology and velocity field of the outflow. The velocity field is found to be described by a "Hubble" law to a remarkable degree of precision over the entire extent of the bipolar outflow. The general characteristics of the velocity field and spatial shape of its red-shifted lobe are highly suggestive of a bow-shock propagating into a medium with an outwardly decreasing density gradient. Overall, the observations of the spatial-velocity fields of both lobes of the bipolar flow strongly suggest that the underlying agent driving the molecular gas in it is a fast, energetic jet emanating from the central protostellar source. Striking asymmetries in the distribution of low velocity flow material in the two lobes suggest an intrinsic asymmetry in the structure of the ambient gas into which the bipolar flow is propagating. Improved estimates of the outflow's mass, size and energetics are made providing strong constraints on the driving engine.

Key words: ISM: JETS AND OUTFLOWS — STARS: FORMATION

1. INTRODUCTION

The generation of an energetic molecular outflow is a fundamentally important stage of protostellar evolution (e.g., Lada & Shu 1990). Yet, despite more than 15 years of study, the nature of this intriguing

phenomenon is still poorly understood. Although relatively rare, highly collimated bipolar molecular outflows provide particularly important laboratories for investigation of this phenomenon since their special geometry poses significant constraints on the physics of their driving mechanism (e.g., Meyers-Rice & Lada 1991). Detailed study of the spatially resolved velocity fields of such outflows has shown promise for understanding their structure and dynamics (e.g., Cabrit & Bertout 1986, Meyers-Rice & Lada 1991, Masson & Chernin 1993, Raga & Cabrit 1993, Stahler 1994, Bachiller et al. 1995).

The striking collimation of the bipolar outflow known as NGC 2264G makes it a prime candidate for detailed study at high angular resolution. This remarkable outflow was initially discovered in a very thorough survey of the molecular gas contained in the giant cloud associated with NGC 2264 and the Mon OB1 association (Margulis & Lada 1986). The outflow was subsequently found to be very unusual in its high degree of collimation, high velocities, and large mechanical luminosity (Margulis, Lada, & Snell 1988). However, most intriguing of all was the lack of a detectable driving source observable at near- and far-infrared wavelengths (Margulis et al. 1990). Given the relatively large velocities and kinetic luminosity of the outflow, the lack of a stellar driving source luminous enough to be detected suggested an extremely efficient driving mechanism for the outflowing molecular gas. Since the first observations of NGC 2264G were made, a growing number of similarly highly collimated, efficiently driven bipolar outflows have been discovered (e.g., Bachiller & Gómez-Gonzalez 1992). Many of these appear to be driven by protostellar objects with extremely "cold" spectral signatures (i.e., so-called "extreme Class I" or Class 0 sources; Lada 1990, Andre, Ward-Thompson, & Barsony 1993). Similar to the driving source of NGC 2264G, these sources were not typically detected at near-infrared or most far-infrared wavelengths. However, until recently, the nature of the stellar source responsible for producing NGC 2264G has been a mystery. Now, nearly 10 years after the discovery of NGC 2264G, its driving source has been finally identified with VLA observations (Gómez et al. 1994) and confirmed as a Class 0 type source at submillimeter wavelengths (Ward-Thompson, Eiroa, & Casali 1995). Thus NGC 2264G should no longer be regarded as a singular object but instead as a representative of a (rare) class of outflow sources which are associated with young stellar objects in what may be a very early stage of protostellar evolution. Indeed, NGC 2264G is both the oldest and most recent example of the Class 0 phenomenon to be discovered. The nature of the process which produces this unusual outflow activity is, however, still unknown.

In order to improve our overall knowledge of the physical properties and dynamical nature of the NGC 2264G outflow we have performed a detailed study of this source in the $J = 2 \rightarrow 1$ transition of ^{12}CO . The observations were of significantly greater sensitivity than those obtained in previous studies. This, in turn, allowed more accurate estimates of the basic flow properties and permitted us to perform a detailed spatial analysis of the flow's dynamics and energetics. In the remainder of this contribution we present an overview of the initial results of our investigation. The more comprehensive study will be published elsewhere.

2. INSTRUMENTATION

Our CO observations were obtained with the 15 meter JCMT on Mauna Kea Hawaii primarily in October 1992. Supplementary observations were obtained in September 1993. At the observing frequency the telescope's half-power beam width is about 21 arc sec. The spectrometer for the 1992 observations was an AOS with 2048 channels that provided an effective resolution of 330 kHz corresponding to 0.42 km s^{-1} . During the 1992 observations the system temperature was measured to be in the range between 300-950 K. For the 1993 observations the spectrometer was an autocorrelator with 2048 channels and a channel spacing of only 78 kHz. These data were smoothed to match the resolution of the 1992 observations. The system temperature for the September observations ranged between 650-2250 K. Observations were initially obtained in a 30×8 grid with positions uniformly spaced at 20 arc sec intervals. Additional (1992) observations were obtained in grids with 10 arc sec spacings, at two selected locations one each in the red and blue lobes, respectively. Additional (1993) observations were also obtained in two rows to the east and west of the primary mapping grid along the major axis of the outflow to enable a more extensive major axis position-velocity map for the outflow to be made. In all 380 positions were observed toward the outflow. Data were obtained in the position-switching mode with the off position located 30 arc min east of the reference position of the mapping grid. Typical integration time was 4 minutes. The data were calibrated using the standard hot-cold load technique.

3. OBSERVATIONS

In Figure 1 we have simultaneously plotted maps of the CO emission from both the blue and red lobes of this outflow at three progressively increasing flow velocities. (From examination of a suite of similar maps made with smaller velocity intervals we found the outflow to be symmetric around an LSR radial velocity of

between 4 and 5 km s⁻¹. Since there is a relatively strong (i.e., $T_b \approx 3$ K) and narrow CO emission feature at 4.6 km s⁻¹, we concluded that this corresponds to the rest velocity of the flow system, a conclusion strongly supported by interferometric ammonia observations of the dense core surrounding the driving source (Gómez et al. 1995). Figure 1 cogently illustrates two fundamental characteristics of this bipolar outflow: *First*, there is a clear and systematic increase in flow velocity with distance from the central source, confirming the trend observed in previous Nobeyama observations of the 1→0 transition of CO (Margulis et al. 1990). Indeed, the highest observed velocities occur very near the ends of the two lobes where there is very little low velocity gas, particularly in the blue lobe. *Second*, comparison of the three maps clearly show a systematic increase in flow collimation with flow velocity, a trend also observed in the earlier Nobeyama data. Both these properties of outflow gas are common to other highly collimated flows (e.g., Moriarty-Schieven & Snell 1988, Walker et al. 1988, Meyers-Rice & Lada 1991, Richer, Hills, & Padman 1992). These maps also show features not observed previously. In particular, the spatial distribution of emitting gas displays a high degree of symmetry around the origin of the bipolar flow with the two lobes having nearly equal maximum extent in space and velocity. From end to end the outflow extends along the major axis approximately 2.2 pc and our observations have revealed the blue lobe to be roughly twice as extended as indicated in the previous Nobeyama maps. The high degree of symmetry exhibited in the two lobes does not apply to all properties of the flow. Despite their very similar

The NGC 2264G Bipolar Outflow

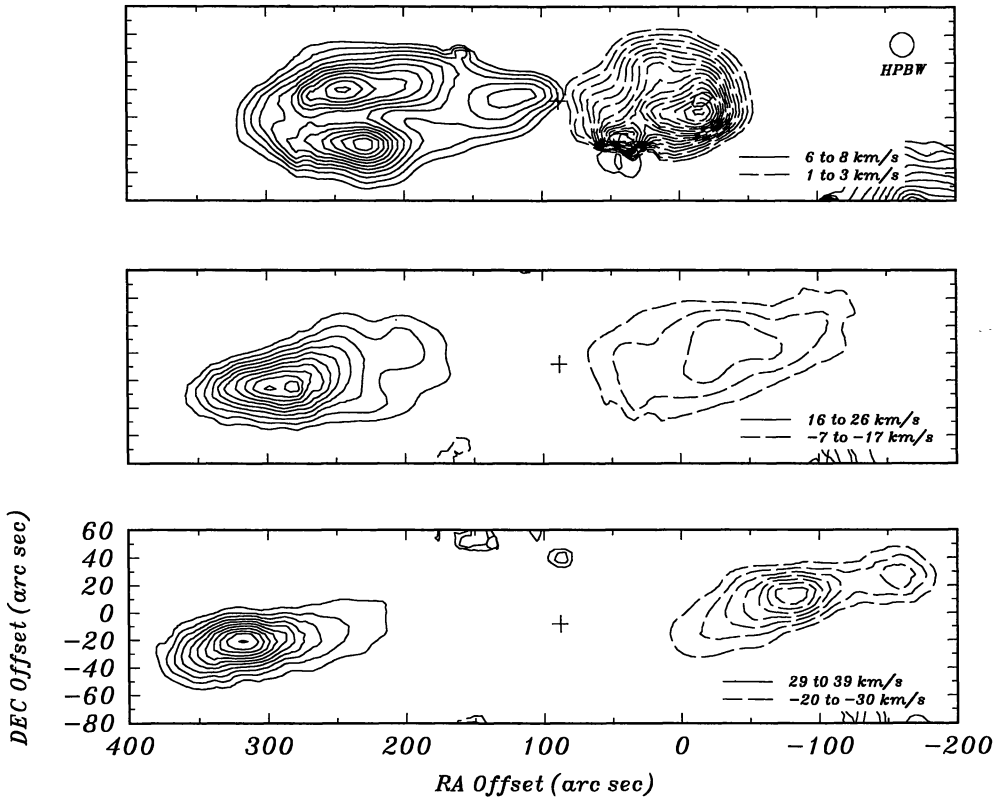


Fig. 1.— Spatial contour maps of the ^{12}CO ($J=2\rightarrow 1$) emission from the NGC 2264G bipolar outflow at three progressively increasing flow velocities. The solid lines correspond to CO emission in the red-shifted lobe and the dashed lines to emission in the blue-shifted lobe of the bipolar flow. The angular resolution of the observations is represented by the circle in the upper right corner of the first panel. The location of the driving source is marked by a cross. These maps illustrate two important properties of the velocity field of the outflow: 1) the systematic increase of flow velocity with distance from the driving source and 2) the progressive increase of flow collimation with increasing flow velocity and distance from the central source.

sizes and extents, the emission from the red lobe is generally brighter than that from the blue lobe and this asymmetry is particularly apparent at intermediate flow velocities. Finally, at low velocities our observations resolve the red lobe into a structure that appears to have the shape of a large bow shock.

4. A "HUBBLE-LIKE" FLOW

The position-velocity (pv) map constructed from spectra observed along the major axis of the flow is displayed in Figure 2. This map reveals a velocity field rich in structure both in the outflow and in the ambient

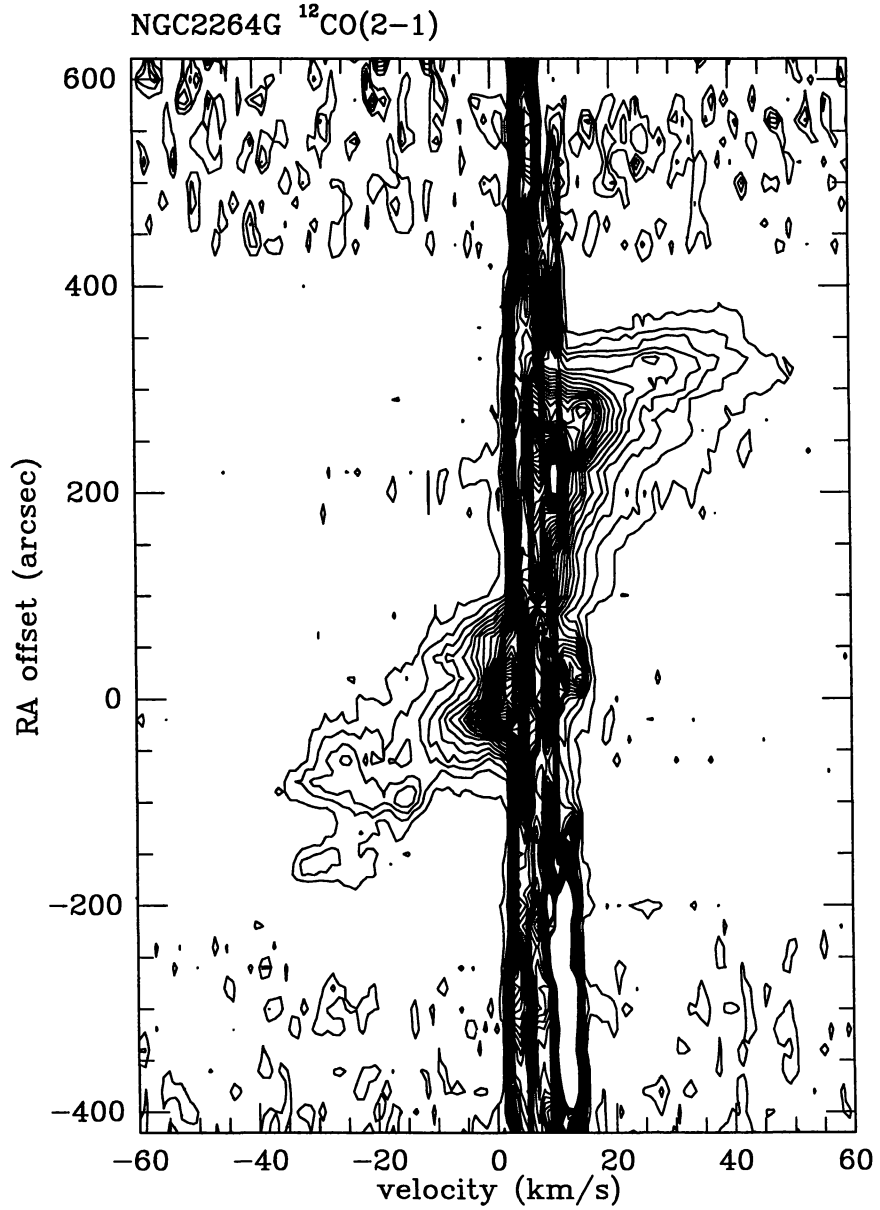


Fig. 2.— The position-velocity map along the major axis of the NGC 2264G outflow. The bipolar velocity field of the outflow is clearly observed. A linear increase in flow velocity with distance from the center of symmetry of the flow appears to characterize the velocity field. Despite the close similarity in both spatial and velocity extent of the outflowing gas, the detailed structure of the velocity fields in the red and blue lobes is strikingly different.

material. Between 4-15 km s⁻¹ multiple velocity features or components can be identified and they make up the "ambient" velocity field. These various components correspond to various individual clouds which make up the NGC 2264 GMC complex. NGC 2264G is near the edge of the NGC 2264 cloud which is located directly west of the flow (at negative RA offsets) in this map. In the vicinity of the outflow the three most prominent ambient components are at velocities of roughly 4.6, 9 and 12 km s⁻¹. The high velocity outflow and its bipolar structure are clearly evident in this map. The extent of the flow in both space and velocity is very nearly the same in both the blue and red lobes reflecting the high degree of symmetry in flow structure observed in the spatial maps (Figure 1). The systematic increase of flow velocity with distance from the central source is particularly clear in the pv map. Indeed, this increase appears to be very linear and "Hubble -like" (especially in the blue lobe) confirming the findings of the earlier observations of this flow (Margulis et al. 1990).

If the velocity field is in fact a "Hubble" flow, then the slopes of the red and blue lobe features (arms) in the pv map give the dynamical time scale and the typical age of the outflowing gas. The dynamical time scale is an important physical parameter of the flow material. It is useful to determine this quantity, not only for the flow as a whole, but also individually for each position in the flow that was observed. Consequently, we calculated the mass-weighted dynamical time, $\langle t_d \rangle$, for each observed position in the blue and red lobes, i.e.,

$$\langle t_d(r) \rangle = r / \langle v \rangle, \text{ where } \langle v \rangle = \frac{\int v T(v) dv}{\int T(v) dv}$$

Here r is the radial distance of the flow element from the central source, $\langle v \rangle$, the temperature (or mass) weighted velocity at that position and T the brightness temperature at a given outflow velocity v . The integration is performed over the velocity range of high velocity gas. This quantity, $\langle t_d(r) \rangle$, is then the temperature or mass weighted dynamical time scale at any given position $\langle r \rangle$ in the flow. In Figure 3 we display the frequency distribution of these timescales in the NGC 2264G outflow. Negative values correspond to measurements in the blue lobe and positive values to measurements in the red lobe. This graph shows that $\langle t_d \rangle$ is a sharply peaked function in each of the lobes. This indicates that the outflow follows the "Hubble-Law" to a high degree of certainty. Evidently, *the dynamical timescale for outflowing gas is essentially the same everywhere in the flow!* The peaks in the histogram in Figure 3 correspond to a dynamical time of 3-4 x 10⁴ years. This should probably be considered an upper limit since we have considered only the projected radial velocity of the flow, not its true velocity. Clearly, any dynamical model for this outflow must be able to predict this robust physical property of the outflow.

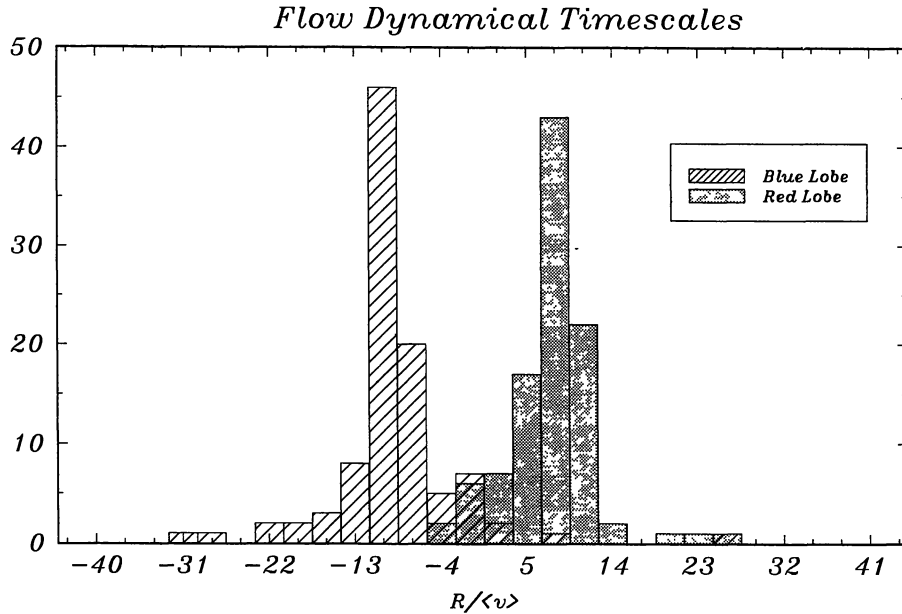


Fig. 3.— Frequency distribution of the mass weighted dynamical time scales. The scale is in 'instrumental' units (i.e., arc sec km⁻¹ sec). To convert to years the conversion factor is 3870. The measurements are strongly peaked at dynamical times corresponding to 3-4 x 10⁴ years and indicate that the flow closely follows a (single) 'Hubble Law' at almost all positions.

5. A LARGE RED BOW SHOCK?

Apart from the close similarity of the red and blue lobes' overall extent in both space and velocity, Figure 2 shows that in certain aspects the detailed structure of their velocity fields is strikingly dissimilar. In particular, the spatial distribution of low velocity material is considerably different in each lobe. Although in both lobes the highest flow velocities are found at the ends of the lobes, there is a marked deficiency of intermediate and low velocity outflow material in the outer regions of the blue lobe compared to the outer regions of the red lobe. This was manifest in the asymmetry of lobe brightness at intermediate velocities observed in the spatial maps of Figure 1. It is also particularly clear in the individual spectra at positions near the end of the blue lobe. These profiles display "detached" line wings, that is, the blue outflow appears as a separate emission line, detached from the emission produced by the ambient gas in the line core. This is very similar to profiles observed in the Mon R2 bipolar flow (Wolf, Lada, & Bally 1992). How is it that a driving engine that produces two lobes of nearly identical spatial and velocity extents, similar masses and energetics (see below) can simultaneously produce such different velocity fields in the lobes? The most likely possibilities are an asymmetry in the underlying wind or jet that sweeps up or entrains the high velocity molecular gas, or an asymmetry in the physical environment that the outflow is propagating in. Although it is not yet possible to conclusively distinguish between these two alternatives, preliminary analysis of our data suggests that the latter may be more likely.

The shape of the red lobe profile in position velocity space results from the fact that along the major axis both high and low velocity outflow material is simultaneously present. This type of pv profile agrees well with that predicted in at least one model describing the entrainment of molecular gas by an underlying fast jet (see Stahler 1994, his Fig. 5). However, this is also similar to what one would expect of material flowing through a bow shock. Moreover, the spatial maps of the flow show that the shape of the red lobe is very close to that predicted by bow shock models in which the shocks propagate into regions of decreasing density gradient (e.g., see Raga & Cabrit 1993, their Fig. 2).

Figure 4 displays maps of the emission in the red lobe at the lowest and highest velocities measurable. The high velocity emission is extremely well collimated and jet-like and extends beyond the edge of the putative bow shock apparently breaking through and preceding it into the ambient cloud. An appealing interpretation of these data is possible in the context of current models of jet driven flows. We suggest that the low velocity gas in the red lobe traces molecular material swept up in a bow shock which is driven by a much faster jet ejected from the central source into an environment with a decreasing density gradient (Raga & Cabrit 1993). The more highly collimated high velocity gas is molecular material entrained close to or at the sides of the underlying jet by some process of turbulent mixing possibly through Kelvin-Helmholtz instabilities at the interface between the jet and ambient gas (Chernin et al. 1994, Stone & Norman 1993a,b).

On the other hand the blue lobe does not show a profile in the pv map that is consistent with jet entrainment or a bow shock. Instead the material in this lobe appears to be moving in a manner that suggests that it is not

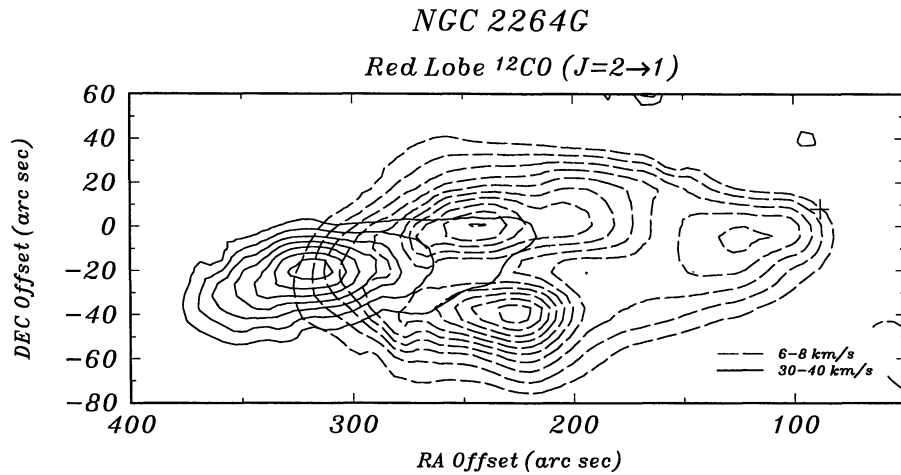


Fig. 4.— Maps of the lowest and highest observable emission from the red lobe of the outflow. The low velocity red lobe material appears to have the structure of a bow shock. The highest velocity red lobe material is highly collimated and jet-like. This jet appears to extend beyond the edge of the bow shock.

significantly entraining or sweeping up surrounding ambient gas. Still, the relatively large mass of this lobe (see below) indicates that the material in it is swept-up ambient gas. But it is possible that this material was at one time swept up near the origin of the flow and has since broken out of the cloud freely moving into a relatively low density region in a ballistic like fashion.

Overall, our observations of NGC 2264G appear to suggest that a fast, energetic jet is the most likely candidate for the underlying wind that drives the molecular outflow. Our current interpretation of the structure and nature of the flow is still rather qualitative and will likely be revised with more detailed and quantitative modeling of the source. In particular, the dynamical origin of the high velocity molecular gas is still poorly understood. Current models have not yet reached a consensus about the detailed physics responsible for sweeping up ambient material into a bipolar molecular flow. Observations, as detailed as those described here, should be extremely useful in aiding the identification of the actual mechanism involved.

6. ENERGETICS

At each location in the flow we have separately calculated for the red and blue lobes the basic energetic parameters using the following integrals:

$$C_1(n) \int_{lobe} v^n T(v) dv \quad \text{and} \quad C_2(n) \int_{lobe} \frac{v^n T(v)}{r} dv$$

Here v is the velocity of the element of gas, $T(v)$, the brightness temperature of the gas at that velocity and r the radial distance from the central source. The flow mass and momentum at each location are calculated from the first integral by setting n equal to 0 and 1, respectively. The flow mass flux, thrust (momentum flux) and mechanical luminosity (energy flux) are calculated from the second integral by setting n equal to 1, 2 and 3, respectively. In both cases $C(n)$ is the appropriate scaling constant. The results are shown in Table 1.

The parameters of the red lobe are underestimates due to the fact that the low velocity (bow shock) gas was excluded from the integrations because of contamination due to ambient cloud material at those velocities. However we do estimate that the mass of low velocity ($6-12 \text{ km s}^{-1}$) material in the red lobe is $0.5 (\pm 0.02) M_\odot$, slightly larger than the mass contained in the higher velocities ($12 - 50 \text{ km s}^{-1}$). The total mass of the outflow is therefore about 1.3 solar masses. In addition in calculating all the quantities other than mass, we have used the (projected) radial velocity not the true total velocity of the material and this leads to additional underestimates of the energetic properties.

Table 1.— Mass and Energetics of the Outflow

Lobe	Mass	Momentum	Mass Flux	Thrust	Mechanical Luminosity
	M_\odot	$M_\odot \text{ km s}^{-1}$	$M_\odot \text{ yr}^{-1}$	$M_\odot \text{ km s}^{-1} \text{ yr}^{-1}$	L_\odot
Red	0.4	5.9	0.8×10^{-5}	1.4×10^{-4}	0.5
Blue	0.4	4.1	0.7×10^{-5}	1.2×10^{-4}	0.5
Total	0.8	10.0	1.5×10^{-5}	2.6×10^{-4}	1.0

Overall our mass and momentum estimates are the most robust and accurate quantities we have calculated. The statistical uncertainties in these quantities are well below 10%. In particular the observed momentum, being a strictly conserved quantity, places strong constraints on the energetics of the flow since it represents a record of the accumulated total momentum that was injected into the flow by the central engine over the flow's lifetime. For example, if the flow has been reasonably steady then we can determine the amount of mass that has been ejected into the underlying driving wind by the central source (Masson & Chernin 1994): $m_{wind} \approx mv_{flow}/v_{wind}$. For NGC 2264G this mass is roughly $0.025 - 0.05 M_\odot$ for typical wind velocities of $200-400 \text{ km s}^{-1}$. This is an appreciable fraction of the mass of the central protostellar object, which given its luminosity of about $12 L_\odot$ (Ward-Thompson et al. 1995), is probably no greater than about $0.5 M_\odot$. If the outflow is powered by accretion onto the central protostar then we expect that the mass accretion and wind mass-loss rates are related through an efficiency factor f (e.g., Shu et al. 1988), and integrating over time we find:

$$\int f \dot{m}_{accretion} dt = \int \dot{m}_{wind} dt \rightarrow f = \frac{m_{wind}}{m_{protostar}} \approx 0.05 - 0.1!$$

This implies an incredibly efficient driving engine. A high efficiency is also indicated by the ratio of the mechanical energy of the flow to the bolometric luminosity of the central source which we find to be > 0.08 . The inequality is due to the fact that the mechanical energy of the flow is not a conserved quantity, particularly if the flow is momentum driven. Since the luminosity of the central protostellar source must be greater than or equal to its accretion luminosity, the outflow energy we measured must be therefore an appreciable fraction of the accretion energy. The large outflow momentum supply rates derived from our observations also place strong constraints on the stellar mass loss rates which supply the underlying jet. For a steady flow we estimate that $\dot{m}_{wind} \approx 0.62 - 1.2 \times 10^{-6} M_{\odot} \text{yr}^{-1}$. The required amount of momentum injection cannot be supplied by a typical optical ionized jet unless it contains a substantial neutral component.

7. CONCLUDING REMARKS

From our initial analysis of a detailed and well-resolved map of the CO emission in this highly collimated outflow we have significantly improved determinations of its mass, size and energetics. In addition, we have identified a number of interesting physical characteristics which may provide potentially important constraints for understanding the dynamical nature of this spectacular bipolar molecular outflow. In particular, we find the velocity of the outflow to increase in a systematic, linear fashion with distance from the central source providing a convincing confirmation of trends observed in earlier studies. Moreover, we find that the detailed structure of the velocity field is described by a "Hubble" ($v \propto r$) law to a remarkable degree of precision over the entire extent of the outflow. We also find that the collimation of the outflow increases systematically with flow velocity and distance from the central source, again confirming trends observed in earlier studies. At the highest velocities the outflow appears very jet-like. The spatial morphology of the red-shifted lobe at low flow velocities appears to match that predicted for bow shocks propagating in media with outwardly decreasing density gradients. The velocity field of this lobe is very similar to that expected from a bow shock and predicted by at least one jet entrainment theory (i.e., although the maximum flow velocity increases with distance from the central source, at most positions emission from the flow spans a wide range of velocity from low to high values). Together, the jet-like collimation of the highest velocity emission, the location of the highest velocity material at the ends of the lobe, the bow-shock like shape of the red lobe at low velocities, and the spatial-velocity signature of the red-shifted gas point to a very fast, mostly neutral energetic jet as the most likely underlying agent which drives the bipolar molecular gas. The overall symmetry of various properties of the individual lobes such as their masses, maximum spatial and velocity extents, mechanical luminosities, and thrusts, suggests that the underlying jet is also characterized by an intrinsic bipolar symmetry which originates very close to the origin of the driving source. On the other hand, the striking dissimilarity of the detailed velocity fields of the two lobes suggests a significant physical asymmetry in the structure of ambient gas into which the lobes are propagating. Finally, we infer that the driving engine of the flow is extremely efficient. In particular, the energy required to drive the molecular outflow is found to be an appreciable fraction of the gravitational accretion energy liberated in the process of forming the central protostellar object.

We thank Colin Masson, Sylvie Cabrit and Jim Stone for enlightening discussions about the nature of bow shocks.

REFERENCES

Andre, P., Ward-Thompson, D., & Barsony M. 1993, ApJ, 406, 122
 Bachiller, R., & Gómez-Gonzalez, J. 1992, A&AR, 3, 257
 Bachiller, R., Guilloteau, S., Dutrey, A., Planesas, P., & Martín-Pintado, J. 1995, A&A, in press
 Cabrit, S., & Bertout, C. 1986, ApJ, 307, 313
 Chernin, L. M., Masson, C. R., Fouveia Dal Pino, E. M., & Benz W. 1994, ApJ, 426, 204
 Gómez, J. F., Curiel, S., Torrelles, J. M., Rodríguez, L. F., Anglada, G., & Girart, J. M. 1994, ApJ, 436, 749
 Lada, C. J. 1990 in The Physics of Star Formation and Early Evolution, ed. C. J. Lada & N. D. Kylafis (Kluwer, Dordrecht), 329
 Lada, C. J., & Shu, F. H. 1990, Science, 248, 564
 Margulís, M., & Lada, C. J. 1986, ApJ, 309, L87
 Margulís, M., Lada, C. J., & Snell, R. L. 1988, ApJ, 333, 316
 Margulís, M. et al. 1990, ApJ, 352, 615
 Masson, C.R., & Chernin, L. 1993, ApJ, 414, 230

Masson, C. R., & Chernin, L. 1994, in *Clouds, Cores and Low-Mass Stars*, ed. D. Clemens & R. Barvainis, ASP Conf. Ser., 65, 350

Meyers-Rice, B., & Lada, C. J. 1991, *ApJ*, 368, 445

Moriarty-Schieven, G. H., & Snell, R. N. 1988, *ApJ*, 332, 364

Raga, A. C., & Cabrit, S. 1993, *A&A*, 278, 267

Richer, J. S., Hills, R., & Padman, R. 1992, *MNRAS*, 254, 525

Shu, F. H., Ruden, S. P., Lada, C. J., & Lizano, S. 1991, *ApJ*, 370, L31

Stahler, S. 1994, *ApJ*, 422, 616

Stone, J. M., & Norman, M. L. 1993a, *ApJ*, 413, 210

Stone, J. M., & Norman, M. L. 1993b, *ApJ*, 420, 237

Walker, C. K., Lada, C. J., Young, E. T., & Margulis, M. 1988, *ApJ*, 332, 335

Ward-Thompson, D., Eiroa, C., & Casali, M. 1995, *MNRAS*, in press

Wolf, G., Lada, C. J., & Bally, J. 1990, *AJ*, 100, 1892